Organic Electronics 30 (2016) 225–236

Contents lists available at ScienceDirect

Organic Electronics

journal homepage: www.elsevier.com/locate/orgel

Critical light instability in CB/DIO processed PBDTTT-EFT:$PC_{71}BM$ organic photovoltaic devices

Andrew J. Pearson [a], Paul E. Hopkinson [a, b, c], Elsa Couderc [a], Konrad Domanski [a, 1], Mojtaba Abdi-Jalebi [a], Neil C. Greenham [a, *]

[a] Cavendish Laboratory, J.J. Thomson Avenue, Cambridge CB3 0HE, United Kingdom
[b] Centre for Advanced Materials, Universität Heidelberg, Heidelberg 69120, Germany
[c] Kirchhoff-Institut für Physik, Universität Heidelberg, Heidelberg 69120, Germany

ARTICLE INFO

Article history:
Received 2 October 2015
Received in revised form
18 December 2015
Accepted 20 December 2015
Available online 8 January 2016

Keywords:
PBDTTT-EFT
PC71BM
OPV
Lifetime
Solar
Instability

ABSTRACT

Organic photovoltaic (OPV) devices often undergo 'burn-in' during the early stages of operation, this period describing the relatively rapid drop in power output before stabilising. For normal and inverted PBDTTT-EFT:$PC_{71}BM$ OPVs prepared according to current protocols, we identify a critical and severe light-induced burn-in phase that reduces power conversion efficiency by at least 60% after 24 hours simulated AM1.5 illumination. Such losses result primarily from a reduction in photocurrent, and for inverted devices we correlate this process in-situ with the simultaneous emergence of space-chare effects on the μs timescale. The effects of burn in are also found to reduce the lifetime of photogenerated charge carriers, as determine by in-situ transient photovoltage measurements. To identify the underlying mechanisms of this instability, a range of techniques are employed ex-situ to separate bulk- and electrode-specific degradation processes. We find that whilst the active layer nanostructure and kinetics of free charge generation remain unchanged, partial photobleaching (6% of film O.D.) of PBDTTT-EFT:$PC_{71}BM$ occurs alongside an increase in the ground state bleach decay time of PBDTTT-EFT. We hypothesise that this latter observation may reflect relaxation from excited states on PBDTTT-EFT that do not undergo dissociation into free charges. Owing to the poor lifetime of the reference PBDTTT-EFT:$PC_{71}BM$ OPVs, the fabrication protocol is modified to identify routes for stability enhancement in this initially promising solar cell blend.

1. Introduction

Organic photovoltaic (OPV) devices are among a number of technologies for solar energy conversion using solution-processed materials. The unstabilised power conversion efficiency (PCE) of OPVs has increased rapidly in the past decade [1], with values of 9–11% now being attained for single- and multi-junction devices [2–4]. These promising figures of merit have resulted from the combined development of novel semiconductors and device architectures that have been optimised for efficient light harvesting [5–7]. Of equal importance to the commercialisation of OPVs is the need to understand and maximise operational stability [8,9]. From these latter studies, a complex picture of degradation emerges, highlighting both environmental effects [10,11] and the interdependence between different materials combinations (semiconductors, interface materials and electrodes) in determining the stability of a working solar cell [9]. One of the key technical challenges to overcome in the realisation of efficient and stable OPVs is to minimise detrimental effects that arise from the so-called 'burn-in' phase, this period describing the relatively fast and often significant loss in device efficiency during the early stages of operation. Although a large number of comparative studies exist where OPV cell stability is improved via materials substitution [9], relatively few have considered the burn-in phase in detail. Arguably, the most studied system to date is the bulk-heterojunction (BHJ) polycarbazole:fullerene blend PCDTBT:PCBM [12–15]. Within this body of literature, Peters et al. demonstrated an apparent insensitivity of PCDTBT:PCBM device stability to electrode choice, when aged under sulphur lamp illumination [13,16]. Instead, the burn-in

* Corresponding author.
E-mail address: ncg11@cam.ac.uk (N.C. Greenham).
[1] Present address: Laboratory of Photonics and Interfaces, Department of Chemistry and Chemical Engineering, Swiss Federal Institute of Technology, Station 6, CH-1015 Lausanne, Switzerland.

http://dx.doi.org/10.1016/j.orgel.2015.12.024

phase was correlated with the creation of states within the bandgap of PCDTBT:PCBM which act to increase energetic disorder, a result that is in qualitative agreement with a study on KP115:PCBM [15]. Further insight into the effects of burn-in was provided by Tournebize et al. who studied photoinduced cross-linking between PCDTBT and PCBM in a thin-film geometry [12,17]. There, the timescales involved were found to be commensurate with the burn-in phase of devices employing the same semiconductors, suggesting a possible formation mechanism for the sub-bandgap states [13]. It is important to acknowledge that following burn-in, the long term stability of such devices remains very promising, with reports of almost no loss in PCE over several thousand hours [16,18,19]. To reduce burn-in losses in PCDTBT:PCBM, purification of high-molecular-weight PCDTBT [14] and light soaking of the organic semiconductor blend film during device fabrication [20–22] have been independently demonstrated as effective strategies, the latter also imparting improved thermal stability. These studies not only highlight the complex nature of the burn-in phase but also the non-trivial process of obtaining a meaningful physical understanding which can provide the necessary feedback for rational semiconductor synthesis and device construction, thereby realising efficient and stable OPVs.

In this article we characterise the burn-in phase of OPV devices incorporating a derivative of PTB7, advancing our understanding of solar cells with initially high PCE. The PTB family of copolymers have emerged as promising candidates for high-performance OPVs [23], with devices incorporating PTB7:$PC_{71}BM$ having some of the highest certified efficiencies for single-junction solar cells (~9%) [1]. To achieve these values, a common step in the preparation of the active layer is the use of diiodooctane (DIO) as an additive in the organic semiconductor blend ink, which mediates the drying process of the film [24] to impart a favourable nanostructure for photocurrent generation [25,26]. This general approach has been adopted for a large number of polymer:fullerene solar cells [27], with DIO being the most popular additive. There have however been few stability studies on PTB7-based solar cell devices [2,28–30], with the majority concerned with storage stability only [2,29–31]. A low-bandgap derivative of PTB7, PBDTTT-EFT (also known as PTB7-Th or PCE-10) has been recently synthesised to further increase the efficiency of OPVs [32,33], with uncertified reports of up to 10% PCEs from manufacturers [34]. Motivated by the absence of lifetime data this material forms the basis of our study, where we evaluate the performance of PBDTTT-EFT:$PC_{71}BM$ BHJ devices during extended simulated AM1.5 solar illumination. By measuring unencapsulated devices under nitrogen, the limiting factors in solar cell stability are determined. The unique aspect of our setup is the ability to monitor in-situ the electrical properties of a solar cell using transient photocurrent (TPC) and transient photovoltage (TPV) techniques, alongside standard current–voltage (IV) measurements. This approach provides deeper insight into the evolution of charge-carrier transport, lifetime and recombination during device operation than can otherwise be obtained through analysis of the solar cell short circuit-current density (J_{SC}), open-circuit voltage (V_{OC}) and fill factor (FF).

The presentation and discussion of our results proceeds as follows. We first consider the initial (i.e. unstabilised) efficiencies of PBDTTT-EFT:$PC_{71}BM$ OPVs in both a normal and inverted device architecture. The stability of these devices (the 'reference cells') under nitrogen is then monitored throughout 70 hours simulated solar illumination, this period providing sufficient time for the devices to undergo burn-in before stabilising. Sequential IV, TPC and TPV measurements provide a relatively detailed insight into the photovoltaic properties of the solar cells and from this dataset we provide an initial description of device evolution. We move on to characterise degraded PBDTTT-EFT:$PC_{71}BM$ devices and thin films ex-situ using a range of structural and optical measurements. These results are discussed in the context of our in-situ data to develop a comprehensive understanding of how this OPV system degrades under simulated sunlight. Our study concludes by considering engineering strategies for improving cell photostability.

2. Methods

2.1. Materials and solvents

PBDTTT-EFT/PCE-10 was purchased from 1-Material (product # OS0100). $PC_{71}BM$ (95%) was purchased from Ossila Ltd. Chlorobenzene (99.8%, anhydrous), 1,2-dichlorobenze (99%, anhydrous) and DIO (98%) were purchased from Sigma–Aldrich (product #s 12345, 240664 and 250295 respectively). All materials and solvents were used as received without any further purification.

2.2. Sample preparation

ITO-coated glass substrates (Colorado Concept Coatings) were cleaned in warm acetone and 2-propanol in an ultrasonic bath before use. For inverted architecture devices, after drying the clean substrates with compressed nitrogen, a layer of compact TiO_2 was deposited via spin-coating a precursor solution of Titanium Isopropoxide (99.999%, Sigma–Aldrich) (7 vol% EtOH with 0.7 vol% 2M HCl) at 2000 rpm. Substrates were subsequently annealed at 420 °C for 30 min under ambient conditions, slowly cooled to room temperature and transferred to a dry glovebox environment. Note that the sheet resistance of ITO increases from 15 Ω/sq to 40 Ω/sq due to this process. The resulting TiO_2 film thickness was ~35 nm. For normal architecture devices the same substrate cleaning protocol was followed. A layer of PEDOT:PSS (Heraeus Clevios™ AI4083, pre-filtered using a 0.45 μm PVDF filter) was deposited via spin-coating at 5000 rpm to give a layer thickness of ~35 nm. Post-deposition annealing was carried out at 130 °C for 10 min under ambient conditions. PBDTTT-EFT, dissolved at 10 mg ml^{-1} in chlorobenzene or chlorobenzene:1,2-dichlorobenzene (1:1 by vol%), was added to dry $PC_{71}BM$ powder to create a blend solution with a PBDTTT-EFT:$PC_{71}BM$ blend ratio of 1:1.5 by weight and a total solid concentration of 25 mg ml^{-1}. DIO was added to the chlorobenzene ink at 3 vol%. Blend solutions were placed on a hot plate held at 70 °C overnight to encourage dissolution of solid material and cooled before use. TiO_2 or PEDOT:PSS coated substrates were cleaned via spin-coating neat chlorobenzene prior to deposition of the PBDTTT-EFT:$PC_{71}BM$ blend ink. All blend thin-films were prepared via spin-coating at 3000 rpm for 180 s, with a methanol wash applied during the final 30 s. The resulting photoactive layer had a thickness of ~110 nm as determined using spectroscopic ellipsometry. Films were transferred within the glovebox to a vacuum chamber, where a bilayer back electrode of MoO_x (10 nm) and Ag (100 nm) (for inverted devices), or Ca (10 nm) and Ag (100 nm) (for normal devices) were deposited via thermal evaporation through an 8-pixel mask (typical deposition rates and vacuum pressures were 0.1 nm s^{-1} and 1×10^{-5} mbar respectively). The overlap between device anode and cathode defined an active area of 0.045 cm^{-2}. Films for ex-situ characterisation were prepared according to the same methods as complete solar cell devices.

2.3. Characterisation

2.3.1. PCE/EQE

PCE measurements were made on encapsulated solar cells under ambient conditions. Performance was characterised using an ABET Sun 2000 AM 1.5 G solar simulator and Keithley 2635 source

measure unit (SMU). Light output was calibrated using a Si reference photocell to 100 mW cm^{-2}. EQE spectra were acquired using a custom setup using a 100 W tungsten lamp light-source and monochromator. A Thor Labs SMR05 silicon photodiode with known spectral response was used to calibrate EQE values of the PBDTTT-EFT:$PC_{71}BM$ cells. Data are presented after correction of the solar simulator output for spectral mismatch.

2.3.2. In-situ IV, TPC and TPV

To minimise device degradation, solar cells were loaded into a purpose built sample atmospheric chamber (with a capacity for four devices) within the glovebox before measurement. During each experiment the chamber was held at a slight overpressure of continuous dry nitrogen flow, which was filtered (SGT Super Clean) to minimise residual oxygen, moisture and hydrocarbon content. Oxygen and water content was monitored in-situ using a gas analyser (Rapidox 3100D – Cambridge Sensotec) connected to the gas exit line of the sample chamber. A Newport Solar Simulator with equivalent 1 sun output was used for light-soaking the entire device area, with solar cell current–voltage characteristics collected using a Keithley 2636 SMU. A 465 nm LED (LED465E, Thor Labs) was used as the light source for transient experiments, connected to an Agilent 33500B wavefunction generator and purpose-built low-noise PSU. Solar cell transients were recorded by connecting the device to a Tektronix DPO 3032 oscilloscope. For TPC measurements, the device was connected to the 50 Ω input of the oscilloscope via a custom trans-impedance amplifier. The 1 MΩ input of the oscilloscope was used for TPV measurements. An RC time constant of 80 ns was estimated for the solar cells, assuming a geometric capacitance of 1.6 nF (cell area 0.045 cm^{-2}, thickness 100 nm, relative dielectric constant ~ 4). This value is significantly lower than the time resolution of the oscilloscope (2 μs) during TPC measurements. White-light bias for TPV measurements was provided by the solar simulator. A custom written LabView VI was used for instrument control and data acquisition (a looped sequence of IV, TPC, TPV measurements followed by 10 min light soaking).

2.3.3. Optical Spectroscopy

Measurements of sample optical density – referenced to air – were made using a HP 8453 UV–VIS spectrometer in ambient conditions. Raman spectra were acquired using a Horiba T6400 Spectrometer (632 nm HeNe laser excitation source) from films on silicon substrates. Samples were stored under nitrogen during measurement. For PDS measurements, PBDTTT-EFT:$PC_{71}BM$ and TiO_2 films prepared and degraded in an identical fashion to OPV devices were deposited onto Spectrosil quartz slides. Samples were exposed to monochromatic light (the pump), producing a thermal gradient due to the non-radiative relaxation of absorbed light. This results in a refractive index gradient at the sample surface, which is enhanced by immersing the sample in an inert liquid (Fluorinert FC-72) which exhibits high refractive index changes for small variations in temperature. A 670 nm c.w. laser beam (the probe) was passed through this refractive index gradient producing a deflection proportional to the absorbed light. The deflection was measured using a position sensing detector and a lock-in amplifier. Because the deflection is proportional to the light absorption in the sample at that wavelength of the pump, scanning pump wavelength yields a complete absorbance spectrum. UPS data were acquired on TiO_2 films deposited on silicon substrates using a Thermo Scientific ESCALAB 250Xi Photoelectron Spectrometer.

2.3.4. Transient absorption spectroscopy

Samples were excited with ultrafast pulses derived from the output of a 1 kHz regenerative amplifier (Spectra-Physics Solstice), which was used to seed a traveling optical parametric amplifier (TOPAS, Light Conversion) and generate 550 nm pulse with a pulse duration under 200 fs. For pump-probe delays above 2 ns, the samples were excited with the output of a frequency-doubled Q-switched Nd-YVO4 laser (Advanced Optical Technologies) triggered electronically; the excitation wavelength was 532 nm and the pulse duration around 1 ns. The devices were probed in a reflection configuration using the broadband outputs of home-built noncollinear optical parametric amplifiers (600–780 nm and 1100–1200 nm). The probe beam was split to provide a reference signal that measures an area of the sample not excited by the pump, to mitigate the effect of laser fluctuations. The probe and reference signals were dispersed in a spectrometer (Andor, Shamrock SR-303i) and detected using a pair of 16-bit 1024-pixel linear image sensors (Hamamatsu, S8381-1024Q), which were driven and read out at 1 kHz by a custom-built board from Stresing Entwicklunsbuero. Pump and probe polarizations were set to magic angle (54.7°). Devices were held at short circuit unless otherwise stated.

2.3.5. Scanning Probe Microscopy

Samples were measured using a Veeco Instruments Dimension 3000 Scanning Probe Microscope, operating in tapping mode. Tips from MikroMasch were used (HQ:NSC15/AL BS), with a resonant frequency and spring constant of ~325 KHz and ~40 Nm^{-1} respectively. Image analysis was carried out using the Gwyddion software package (http://gwyddion.net/).

2.3.6. X-ray Scattering

Samples were measured in a grazing-incidence geometry at beamline I07 of the Diamond Light Source (Harwell, U.K.). A beam

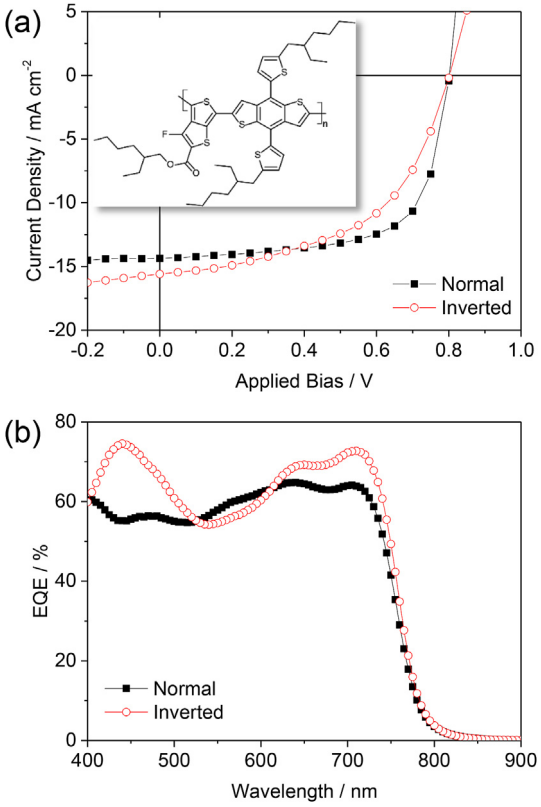

Fig. 1. Steady state photovoltaic characteristics of reference normal and inverted architecture PBDTTT-EFT:$PC_{71}BM$ BHJ solar cell devices. (a) Current density–voltage curves for typical devices under 1-sun equivalent illumination, with the chemical structure of PBDTTT-EFT shown in the inset. (b) External quantum efficiency (EQE) spectra for the same cells.

energy of 10 keV was used with samples housed in a custom-built chamber during measurement. Samples were tilted at 0.16° into the path of the incident X-rays. X-ray scatter was measured using a Pilatus 2M detector, calibrated using silver behenate powder. Collected data was analysed using the DAWN software package (http://www.dawnsci.org/).

3. Results and discussion

3.1. Initial solar cell performance and lifetime data

In Fig. 1 we present the initial photovoltaic characteristics of PBDTTT-EFT:$PC_{71}BM$ BHJ solar cell devices processed using chlorobenzene solvent and DIO as a processing additive [32,33].

Reference solar cells were fabricated either in an inverted architecture, ITO/TiO_2/PBDTTT-EFT:$PC_{71}BM$/MoO_x/Ag, or a normal architecture, ITO/PEDOT:PSS/PBDTTT-EFT:$PC_{71}BM$/Ca/Ag [32]. Because DIO has a high boiling point and a relatively low vapour pressure, small volumes are expected to linger in the polymer:fullerene blend thin film after casting at ambient temperatures. Residual solvent is already known as a source of instability in OPVs [35] and so to counter this specific effect, blend films were washed with methanol after casting to minimise residual DIO content prior to thermal evaporation of the back electrode [36]. Efficient photovoltaic behaviour is obtained for devices fabricated according to this protocol, with inverted and normal architecture devices reaching average efficiencies of 6.0 ± 0.5% (J_{SC} = −15.1 mA cm^{-2}, V_{OC} = 0.79 V, FF = 50%) and 7.3 ± 0.5% (J_{SC} = −14.0 mA cm^{-2}, V_{OC} = 0.8 V, FF = 65%) respectively (the latter exhibiting identical FF and V_{OC} values to previous reports [32]). From Fig. 1 (b), it can be seen that the larger J_{SC} of the inverted solar cell results from the enhanced spectral response in the UV and near-IR regions of the solar spectrum.

The stability of the reference cells was evaluated over 70 hours in an atmospheric chamber under continuous dry nitrogen flow, with typical oxygen and moisture levels of <5 ppm and <30 ppm respectively. The chamber temperature – measured using an internal Pt resistance thermometer placed next to the devices – did not exceed 40 °C, this temperature being reached within 15 minutes of the experiment commencing. An automated routine was developed to enable data collection after every 10 minutes of light soaking, with short (<30 s) intermediate periods of dark storage during collection of TPC data. Solar cells were held at open circuit between current–voltage scans. In Fig. 2, the evolution in solar cell performance is presented, where individual metrics have been normalised to their initial values. For both solar cell architectures a severe drop in PCE is observed, with the largest changes occurring within the first 24 hours. For inverted devices, the relative evolution in individual metrics is presented in Fig. 2 (b), where it can be seen that the short-circuit current undergoes the largest overall reduction (80%) followed by the open circuit-voltage (40%).

For normal architecture devices the short circuit-current also undergoes the largest relative drop (see Fig. 2 (c)). Although the FF for these solar cells undergoes a larger relative drop compared to the inverted devices, the absolute values after stabilising are comparable (40–45%). A control experiment was undertaken in dark conditions to determine the extent to which the trace levels of oxygen and water in the sample chamber atmosphere influence

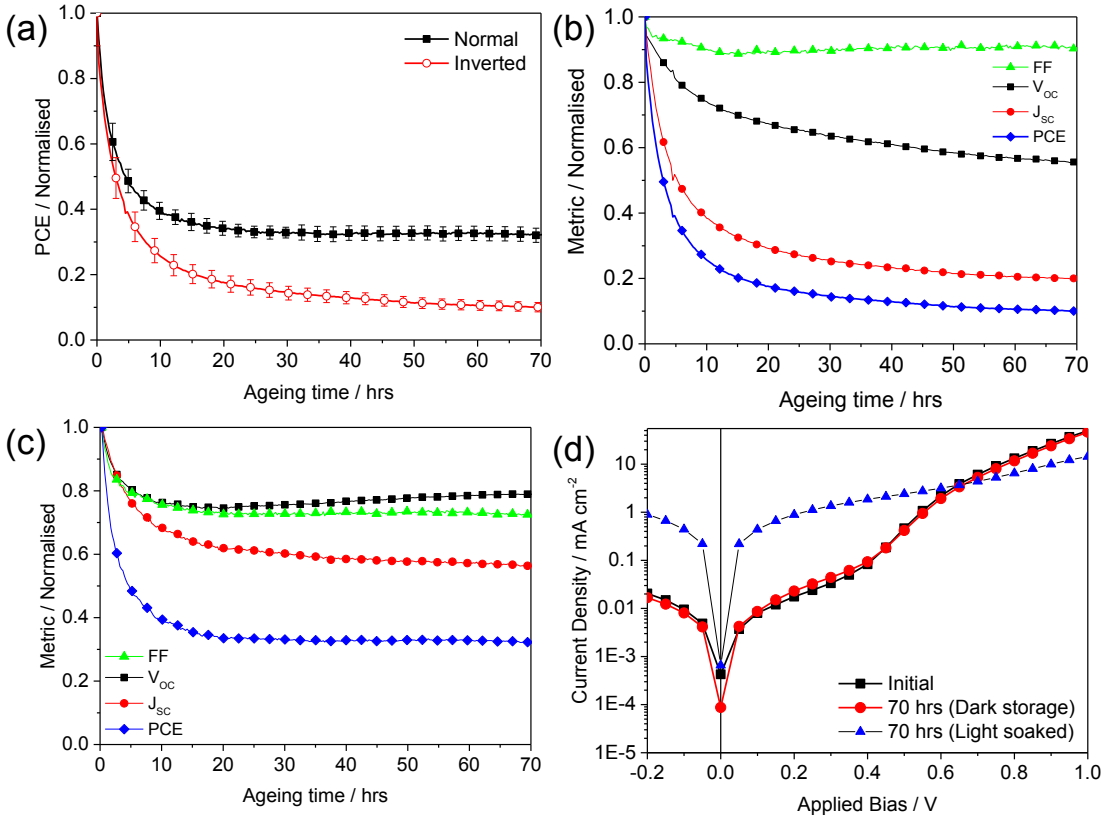

Fig. 2. Performance under continuous simulated solar illumination of PBDTTT-EFT:$PC_{71}BM$ reference cells. (a) Evolution of solar cell efficiency for normal and inverted devices, normalised to their initial values. (b) Evolution of average performance metrics for inverted architecture cells. (c) Evolution of average performance metrics for normal architecture cells. Note that each quantity in (b) and (c) has been normalised to its initial value. (d) Comparison of dark current–voltage behaviour for inverted architecture cells before and after extended dark storage, or after extended light soaking.

device stability. The result of this experiment, presented in Fig. 2 (d), does not show a significant change in diode characteristics over a timescale similar to the original experiment (note that current–voltage scans were collected every 10 minutes as before). In contrast, the dark IV behaviour of the light-soaked device is significantly modified from its initial state. These results tentatively suggest that burn-in in PBDTTT-EFT:$PC_{71}BM$ reference solar cells is dominated by light mediated processes.

3.2. In-situ transient characterisation of performance losses

To gain further insight into the loss of solar cell efficiency, we proceed to discuss the evolution in device performance as characterised through in-situ transient electrical measurements. Specifically, the solar cell response to a 200 μs square-pulse optical excitation from a 465 nm LED was monitored either at short circuit for TPC, or close to open circuit for TPV. The LED brightness (c. 1 mW cm^{-2}) was sufficiently low to ensure that the voltage perturbation during TPV measurements was less than 5% of V_{OC}. The evolution in TPC characteristics for inverted architecture devices (which underwent the largest overall reduction in device efficiency) is presented in Fig. 3. Individual TPC traces can be broadly described according to three regimes of rapid (~μs) rise, adjustment to a quasi-steady-state value, and rapid fall with a tail extending for up to several tens of μs. In general, fast components are often attributed to the transport of mobile charge carriers whereas slower components are attributed to charge trapping/detrapping processes [37].

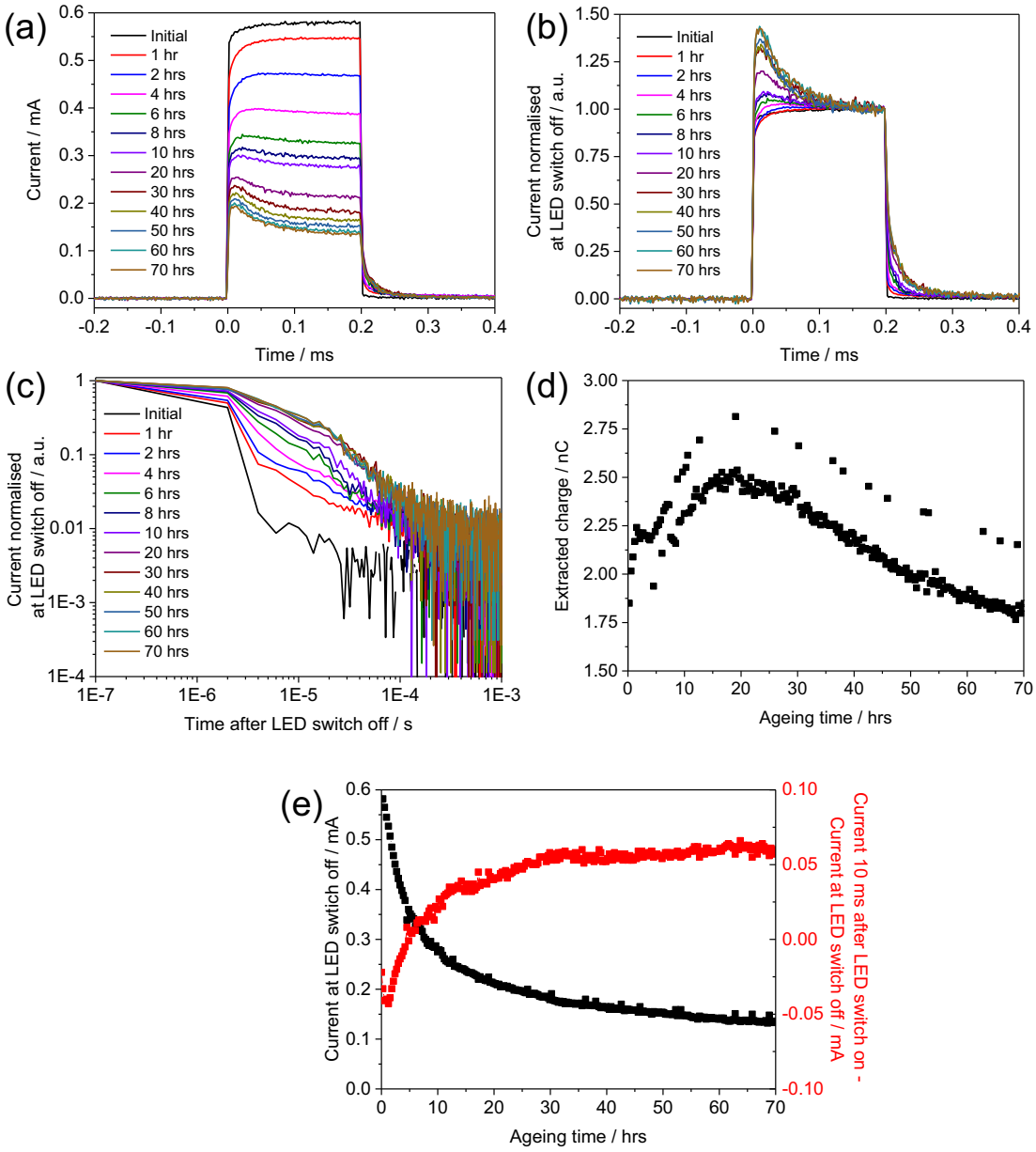

Fig. 3. Evolution of the transient photocurrent (TPC) response from inverted architecture cells during extended simulated solar illumination (t = 0 ms defines the start of the LED pulse). (a) Absolute TPC response at distinct stages of the experiment, with data normalised to the current at LED switch-off presented in (b) (entire data) and (c) (decay kinetics). Note the different time axis presented in part (c). Throughout the entire experiment, the integrated charge from each transient decay is plotted in (d), where intermittent data points corresponding to a higher extracted charge than the trend arise from current fluctuations 40 μs after LED switch-off. In part (e), changes in transient photocurrent at LED switch off (quasi-steady-state) are compared with the current 10 μs after LED switch-on.

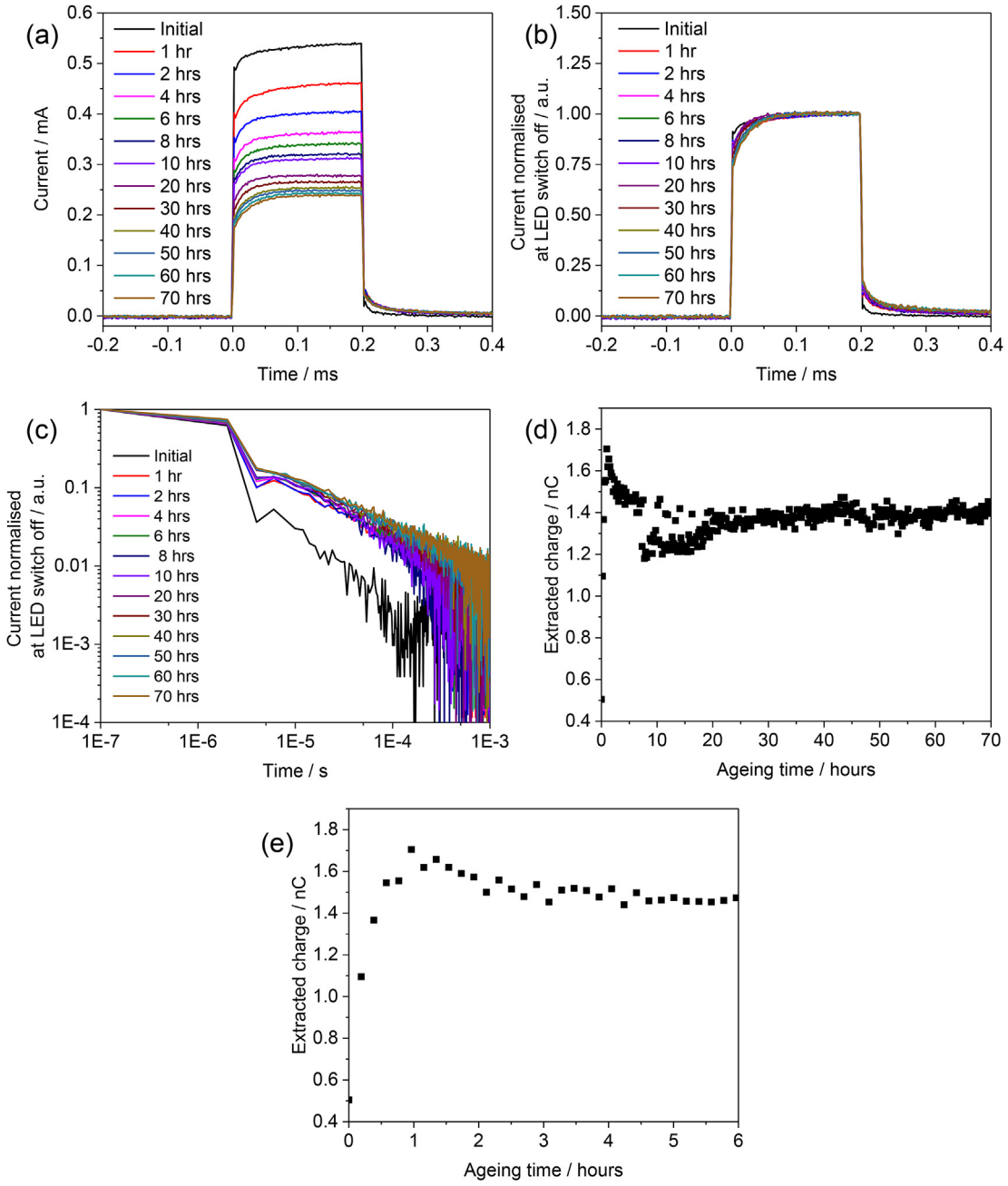

Fig. 4. Evolution of the transient photocurrent (TPC) response from normal architecture cells during extended simulated solar illumination (t = 0 ms defines the start of the LED pulse). (a) Absolute TPC response at distinct stages of the experiment, with data normalised to the current at LED switch-off presented in (b) (entire data) and (c) (decay kinetics). Note the different time axis presented in part (c). Throughout the entire experiment, the integrated charge from each transient decay is plotted in (d) and (e), where part (e) highlights the initial rise in extracted charge during the first hour of ageing.

In Fig. 3 (a) it can be seen that the cell transient photocurrent undergoes a relative reduction with increasing exposure to simulated solar illumination, in agreement with the evolution in device short-circuit current (Fig. 2 (b)). Furthermore, an overshoot in photocurrent begins to emerge almost immediately following LED switch-on, relative to the values at 0.2 ms. In the regime shortly after LED switch-off (t > 0.2 ms), the tail in the TPC signal is measured to decay over progressively longer timescales during the course of the experiment i.e. with increasing degradation of the solar cell. The relative significance of these features is highlighted in Fig. 3 (b)–(c), where each TPC trace has been normalised to its current value at LED switch-off (t = 0.2 ms).

The overshoot in transient photocurrent measurements has previously been observed in bulk-heterojunctions of P3HT:PCBM [38], P3HT:F8BT [38] and polymer:nanocrystal photovoltaic devices [38,39], in addition to PCDTBT:PCBM BHJ devices under applied bias [40]. In each case the overshoot was attributed to a build-up of trapped charge, a process which modulates the internal electric field in the device as it equilibrates with the transport of free charges during steady-state illumination. Photocurrent loss may subsequently occur via recombination of charge carriers, either through trap states or enhanced by space charge effects [40]. A barrier to charge extraction [40-42] – that may be caused by morphological changes in the active layer [42] – can also give rise

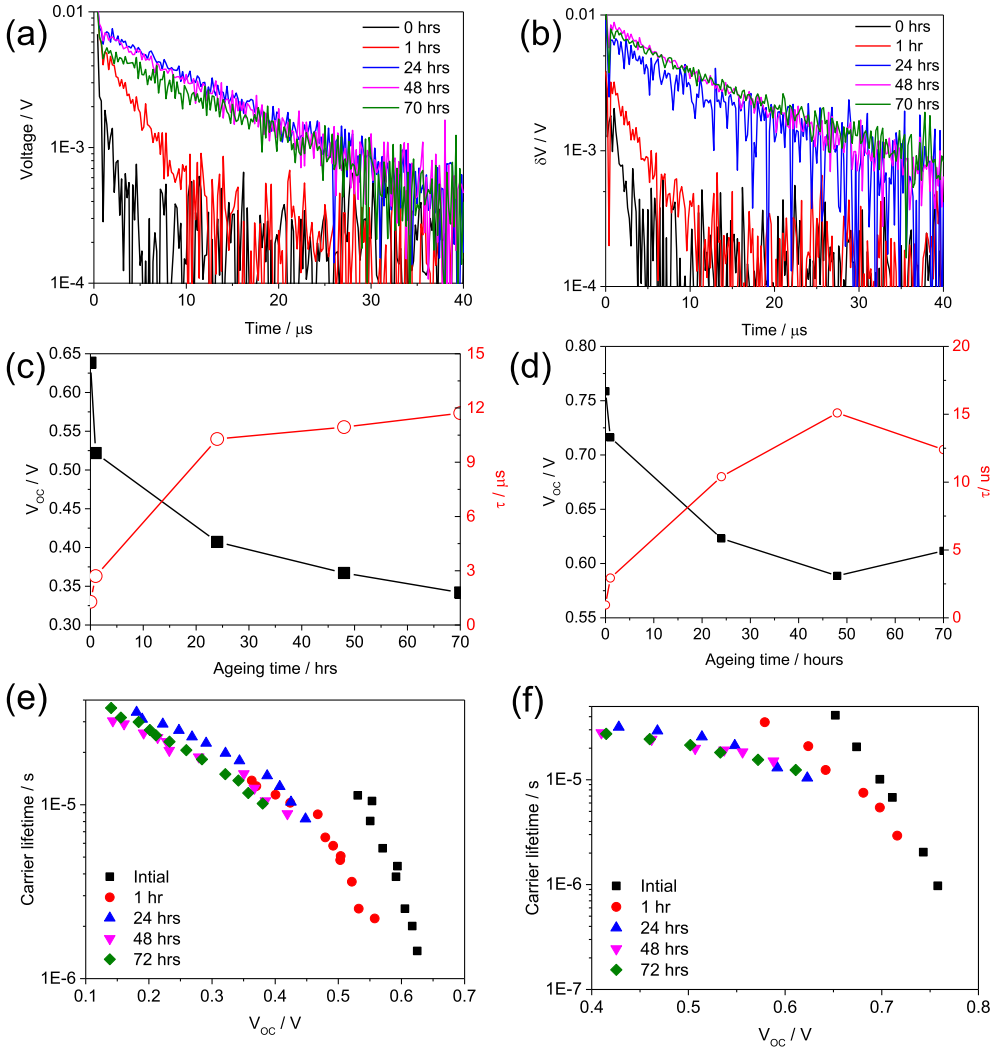

Fig. 5. Evolution in transient photovoltage (TPV) characteristics for reference solar cells as a function of 1 sun light soaking. Voltage transients after subtraction of V_{OC} for (a) inverted devices and (b) normal devices. (b) V_{OC} values overlaid with decay times τ (right axis) for (c) inverted devices and (d) normal devices. Carrier lifetime as a function of V_{OC} for inverted (e) and normal (f) solar cells at different ageing times. To achieve different V_{OC} values, the incident white light bias was varied using a series of neutral density filters.

to this feature. Numerical simulations of P3HT:F8TBT BHJ OPVs have shown that the prominence of the current overshoot during device illumination and the transient decay kinetics can be correlated with the density of trap states and the relative ratio of charge trapping and de-trapping rates within the semiconductor blend [37]. Calculating these values however requires knowledge of both the charge generation rate and the mobility of charge carriers within the solar cell, quantities that are not measured in-situ with our experimental setup.

Regarding the TPC decay kinetics in Fig. 3 (c), it can be seen that degradation increases the time for which current continues to flow from the solar cell after LED switch off. This observation is consistent with a relatively slow charge detrapping process taking place. We note that recent work on aged PCDTBT:$PC_{71}BM$ BHJ OPVs has attributed an increased transient decay signal at relatively short times (<20 μs after LED switch off) to trap states located at the electrode interfaces of the solar cell [43]. Such trap states may also form in the system studied in this work, as we also observe a substantial rise in signal at short times which modifies the global decay dynamics. Indeed, we find that beyond approximately 10 hours into the experiment, a 'kink' emerges 30 μs after LED switch-off, which may suggest two distinct regimes of charge detrapping [37]. The relative significance of bulk and electrode interface degradation behaviour for PBDTTT-EFT:$PC_{71}BM$ OPVs under the conditions explored here is considered later on in our discussion.

In Fig. 3 (d), the integrated current from each transient decay (t > 0.2 ms) is presented as a function of light soaking time. Here, the absolute extracted charge is found to increase at early light soaking times (up to approximately 20 hours) before decreasing. The initial increase is consistent with a greater population of charges becoming trapped within the solar cell during illumination, before detrapping and undergoing subsequent extraction after LED switch off. The measured decrease in extracted charge at later times is potentially counterintuitive and we suggest that this behaviour reflects the development of a process that competes with charge extraction. Specifically, following severe degradation it is possible that relatively deep traps exist within the solar cell from which charges are unlikely to escape from on the ms timescale (i.e. commensurate with the TPC measurement period). Such charges would therefore not contribute to the extracted charge signal which follows LED switch off. We note the close coincidence between the times at which the extracted charge is maximised and when the burn-in phase is approximately complete (see Fig. 2

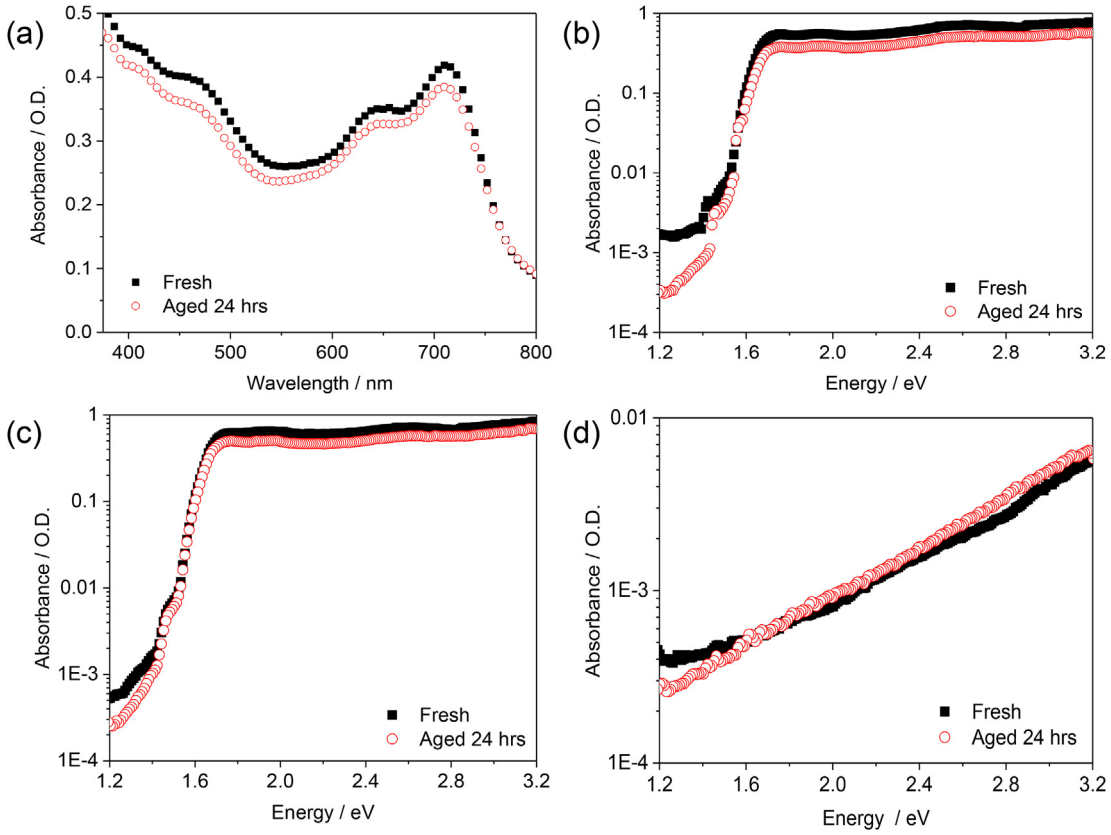

Fig. 6. (a) UV–VIS absorbance spectra for glass/ITO/TiO_2/PBDTTT-EFT:$PC_{71}BM$ before and after 24 hours light soaking from the solar simulator. The absorbance of PBDTTT-EFT:$PC_{71}BM$ deposited on quartz/TiO_2 and blank quartz substrates (as measured using PDS) are presented in (b) and (c) respectively, highlighting the differences in sub-bandgap features that arise due to light soaking. The sub-bandgap absorbance of TiO_2 on quartz is presented in (d). All films were degraded under nominally identical conditions to complete devices.

(b)) and when the dynamics of TPC decay are stabilised (see Fig. 3 (c)), supporting the idea of kinetically distinct periods of device degradation over the course of the entire experiment. Lastly, in Fig. 3 (e) we plot the TPC quasi-steady-state current against the relative prominence of the initial overshoot, here defined as the difference in current at 0.01 ms and 0.2 ms. Because each quantity undergoes a similar evolution due to device burn-in (i.e. the emergence of the overshoot occurs simultaneously with a loss in quasi steady-state photocurrent), we hypothesise that the underlying degradation mechanisms that give rise to these features are closely linked.

The evolution in TPC dynamics for the normal architecture solar cells during ageing is presented in Fig. 4. In qualitative agreement with the data presented in Fig. 3, it can be seen that light induced burn-in also leads to an overall reduction in device photocurrent on the μs timescale. This process does not result in the formation of an 'overshoot' shortly after LED switch on, and we suggest that this difference partly explains why the inverted cells undergo a larger overall reduction in photocurrent with ageing. Instead the loss in photocurrent is correlated with a slower approach to a quasi steady-state value (c.f. normalised data in Fig. 4 (b)). Such behaviour can be rationalised by a faster rate of charge trapping and/or a slower rate of charge detrapping [37], both of which will act to limit the extraction of charge carriers. Concerning the photocurrent decay dynamics (Fig. 4 parts (c)-(e)), we find that the extracted charge reaches a maximum within the first hour of ageing, before decreasing and stabilising after 20 hours.

We now consider the dynamics of both solar cells at V_{OC}. Here, in-situ TPV was performed under 1-sun equivalent white light bias to characterise the charge carrier recombination kinetics at distinct points in the degradation process. These results are presented in Fig. 5. In parts (a) and (b), quasi-steady-state V_{OC} values have been subtracted from individual traces for ease of comparison.

From Fig. 5 (a)–(b) it can be seen that cell degradation results in an increase in charge carrier lifetime time under constant illumination (1 sun equivalent) conditions. Each TPV decay is approximately linear when plotted on a log-linear scale, suggesting that charge carrier recombination is dominated by a single mechanism in this regime [38]. To quantify the decay kinetics we extract a time constant τ by fitting each trace using a single exponential of the form $\delta V = A \exp(-t/\tau)$. Values for τ are plotted as a function of light soaking time in Fig. 5 (c)–(d) alongside quasi-steady-state V_{OC} values. Because τ increases in line with a reduction in V_{OC} over the course of the experiment, from approximately 1 μs–12 μs for each architecture, it is possible that the charge density n within the solar cell has been reduced [44–46]. Although our setup does not permit the direct measurement of n within a solar cell at V_{OC} (e.g. by following the method of charge extraction as described by Shuttle et al. [46]), TPV measurements as a function of white-light bias indicate that at approximately constant V_{OC} faster recombination dynamics occur in the degraded devices relative to their initial states (Fig. 5 (e)–(f)). This result is consistent with the degraded devices exhibiting poor microstructure and/or material energetics for photocurrent generation [43,47] (c.f. Figs. 3–4 and the related discussion on photocurrent loss), assuming that V_{OC} remains a reliable proxy for charge density throughout the conditions explored here.

3.3. Ex-situ structural and optical characterisation of degraded PBDTTT-EFT:$PC_{71}BM$ solar cells

To test our hypothesis, we employ a range of techniques to identify the underlying mechanisms that cause the observed reduction in PBDTTT-EFT:$PC_{71}BM$ reference cell PCE. Specifically, UV–VIS spectroscopy, photothermal deflection spectroscopy (PDS), transient absorption spectroscopy (TAS) were employed ex-situ to characterise the cumulative effects of the burn-in phase (approximately 24 hours). These measurements are complemented by Raman spectroscopy, atomic force microscopy (AFM) and X-ray scattering measurements on the PBDTTT-EFT:$PC_{71}BM$ layer and UV photoelectron spectroscopy (UPS) measurements; the latter used for characterising the cathode interface layer for the inverted devices (TiO_2).

In Fig. 6, the absorbance of PBDTTT-EFT:$PC_{71}BM$ blend films is presented before and after 24 hours simulated solar illumination. As shown in Fig. 6 (a), the shape of the PBDTTT-EFT:$PC_{71}BM$ absorption spectrum remains broadly similar after light soaking. A small (~2 nm) blue-shift in the blend absorption peak initially located at 712 nm is determined, as well as photobleaching (on average 6% between 380 and 800 nm). The magnitude of the photobleach does not in itself account for the loss in J_{SC} (c. 70% drop after 24 hours), motivating further investigation [48]. Complementary measurements of PBDTTT-EFT:$PC_{71}BM$ and TiO_2 absorbance were carried out using PDS to characterise sub-bandgap features that cannot be resolved in a standard UV–VIS experiment. These results, shown in Fig. 6 (b) – (d), confirm that PBDTTT-EFT:$PC_{71}BM$ undergoes photobleaching, this process being apparently independent of the presence of TiO_2 (c.f. parts (b) and (c)). Note that the data in Fig. 6 (b) provide some explanation for the loss in photocurrent of the normal architecture solar cells, as presented earlier in Figs. 2 (c) and 4. PBDTTT-EFT:$PC_{71}BM$ undergoes a loss in absorbance at all energies measured, in contrast to aged films of PCDTBT:PCBM where light soaking was observed to increase sub-bandgap absorbance [13]. For TiO_2 (Eg ~ 3.54 eV – see Supporting Information Fig. S1) an average increase of 7% in sub bandgap absorbance between 1.8 and 3.2 eV is determined (Fig. 6 (d)). Complementary UPS measurements (Supporting Information Fig. S2), do not evidence changes in the work function and valence band positions of the metal oxide, although the signal intensity at the secondary electron cut-off (binding energy = 17.6 eV) is reduced. The PDS data suggest that the formation of sub-bandgap states in TiO_2 may well reflect a small increase in trap density, hindering the extraction of electrons through this layer in a complete solar cell device [49]. To summarise, we interpret our steady-state absorption measurements as an indication that light soaking degrades both the PBDTTT-EFT:$PC_{71}BM$ layer and, to a lesser extent, the TiO_2 cathode interface layer.

Finally, we discuss the differences in solar cell absorption characteristics using TAS over timescales ranging from sub-ps to 0.1 ms, where measurements in the sub-ns regime provide insight into the dynamics of ultrafast charge generation and recombination. Results are presented in Fig. 7. Measurements were conducted on devices held at short circuit using an excitation fluence of 1 μJ cm^{-2}, to minimise non-linear effects that are unlikely to arise under standard solar illumination conditions.

From Fig. 7 (a), it can be seen that the ultrafast dynamics of the transient absorption feature at ~ 1170 nm – attributed to the hole polaron on PBDTTT-EFT – do not change as a result of light soaking. Specifically, both traces include an ultrafast rise that is attributed to free charge generation at a donor–acceptor interface within the time resolution of the setup (~200 fs). The slower component is attributed to free charge generation assisted by the diffusion of photogenerated excitons. The measurements therefore provide an

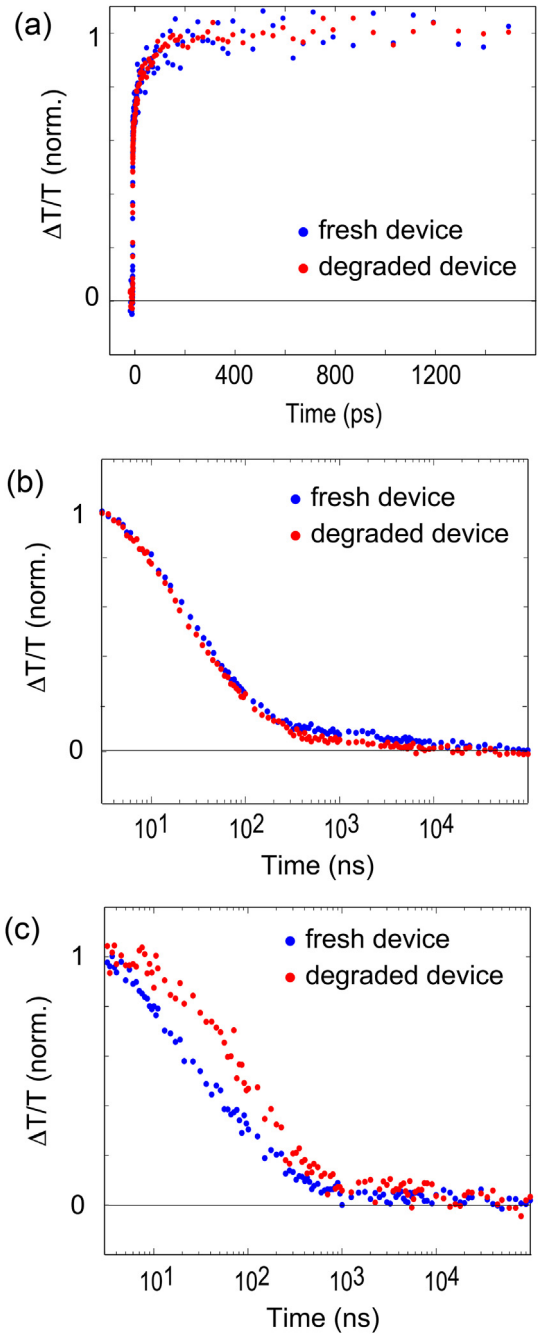

Fig. 7. Transient absorption behaviour of inverted PBDTTT-EFT:$PC_{71}BM$ solar cell devices before and after 24 hours light soaking. (a) Normalised ultrafast dynamics of transient absorption averaged between 1160 and 1180 nm, attributed to the polaron band on PBDTTT-EFT. (b) Normalised long-time dynamics of the polaron band. (c) Normalised long-time dynamics of the PBDTTT-EFT ground state bleach at 750–780 nm.

indirect but sensitive probe of the PBDTTT-EFT:$PC_{71}BM$ BHJ nanostructure. Because no changes are observed in the ultrafast TA kinetics due to ageing, we conclude that light soaking for 24 hours at 40 °C does not drive significant morphological changes in the PBDTTT-EFT:$PC_{71}BM$ blend (e.g. a coarsening phase separation between electron donor and acceptor material that would otherwise modify the balance of ultrafast and diffusion-assisted charge generation). This is supported by AFM and X-ray scattering measurements that do not evidence changes in film structure at length scales above a few nm, as shown in Fig. 8. Specifically, the relative

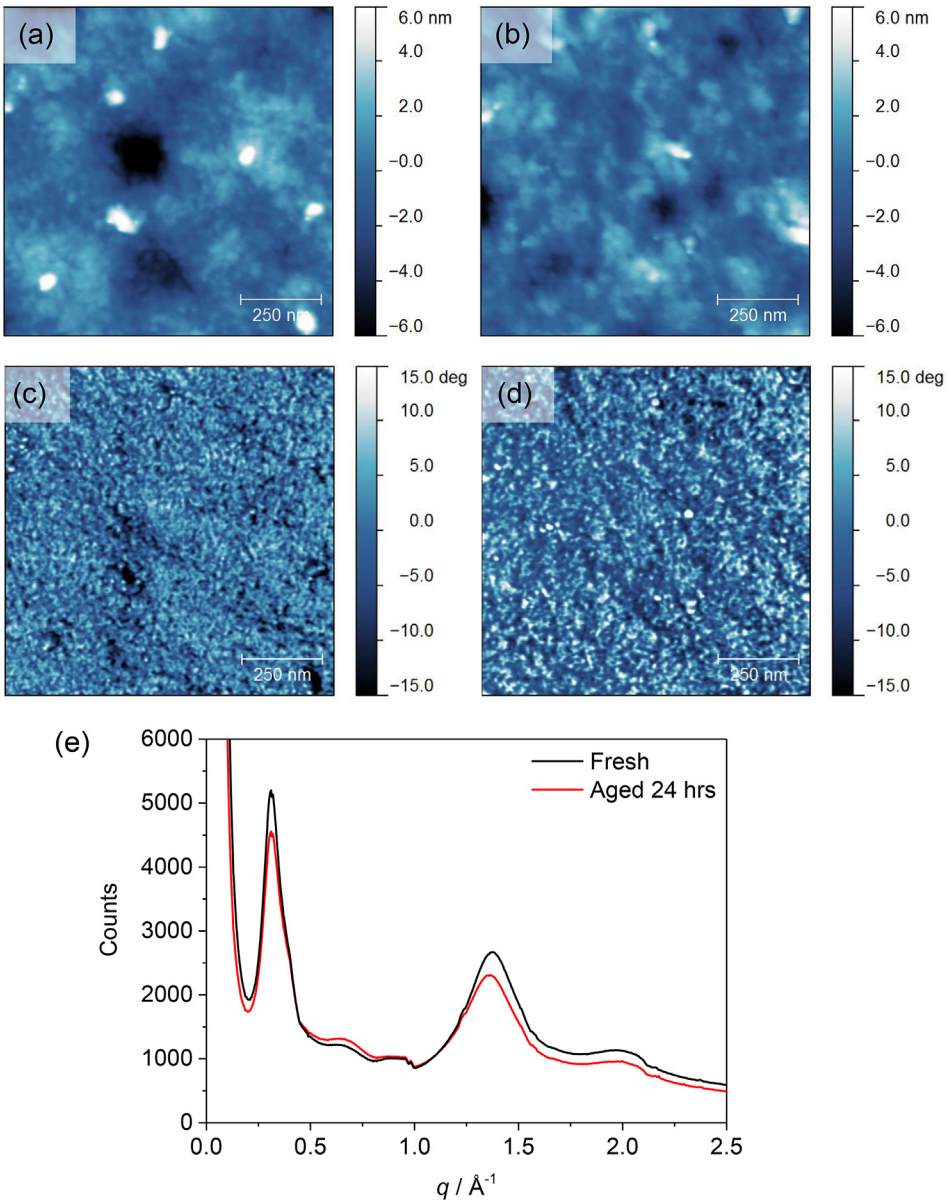

Fig. 8. Comparison of PBDTTT-EFT:$PC_{71}BM$ blend nanostructures before and after 24 hours of light soaking, as measured via tapping-mode scanning probe microscopy and grazing-incidence wide-angle X-scattering (GIWAXS). Parts (a) and (b) show the topography for fresh and light-soaked samples respectively, whilst parts (c) and (d) show the corresponding phase maps. RMS roughness for each surface was <2 nm. GIWAXS measurements (e) indicate that ageing under solar illumination induces a shift of $+0.002$ $Å^{-1}$ in the diffraction peak initially located at 0.317 $Å^{-1}$, and a shift of -0.05 $Å^{-1}$ in the diffraction peak initially located at 1.36 $Å^{-1}$. These peaks are attributed to diffraction of X-rays between adjacent lamella of PBDTTT-EFT chains and adjacent $PC_{71}BM$ molecules respectively.

change in molecular packing between PBDTTT-EFT lamella or adjacent $PC_{71}BM$ molecules is less than 1%. Similarly, the size of polymer- and fullerene-rich domains within the blend thin film also remains stable; a Scherrer analysis of peak widths suggests an approximate domain size of 7.2 nm and 2.3 nm for PBDTTT-EFT and $PC_{71}BM$ respectively, which changes to 7.0 nm and 2.4 nm after 24 hours illumination.

We proceed to discuss the TAS data over the ns − μs timescale, presented in Fig. 7 (b)–(c). Here, the relatively long-time polaron kinetics (Fig. 7 (b)) show that the decay of this signal is unaffected by light soaking. In contrast, changes are observed in the PBDTTT-EFT ground state bleach (GSB) dynamics in the ns − μs time range (Fig. 7 (c)). Specifically, the GSB in the degraded device relaxes over a relatively longer timescale than in the fresh device, with the fresh device exhibiting almost identical polaron and GSB decay kinetics. In the presence of white light background illumination (see Supporting Information Fig. S4), GSB relaxation is modified further, with a full decay requiring tens of μs. The GSB dynamics of fresh devices are not affected by the presence of background illumination, or by placing the device at open-circuit conditions. It is possible that the longer GSB decay time in the degraded device occurs due to relaxation by additional excited state species (deeply trapped charges or triplet states) that do not contribute to the solar cell photocurrent. We hypothesise that the mechanism by which these additional states form is associated with the partial loss of chromophores that results from photobleaching of the PBDTTT-EFT:$PC_{71}BM$ blend layer (see Fig. 6). Although our work to identify these additional excited state species is ongoing, alongside experiments to confirm the exact chemical modifications in PBDTTT-EFT:$PC_{71}BM$ that result in this effect, preliminary measurements using resonance Raman spectroscopy measurements do not evidence significant changes in the Raman

signal between 1400 and 1660 cm^{-1} (see Supporting Information Fig. S5). Here, the peak at 1492 cm^{-1} is attributed to the C=C stretching mode on the BDT unit [50]. At this stage it is important to acknowledge that any additional photochemical reactions involving trace amounts of solvent (CB or DIO) cannot be ruled out.

3.4. Overcoming PBDTTT-EFT:$PC_{71}BM$ photoinstability

Our electrical and spectroscopic measurements have provided a detailed characterisation on the effects of light-induced burn-in for PBDTTT-EFT:$PC_{71}BM$ BHJ solar cells. Under the conditions investigated here, device degradation is a multifaceted process that includes contributions from PBDTTT-EFT:$PC_{71}BM$ and, for the inverted architecture device, TiO_2. At short circuit, photocurrent loss during burn-in is directly correlated with a simultaneous build-up of trapped charge within the solar cell on the μs timescale and an increase in charge extraction time. We further evidence a peak in the amount of charge that can be extracted from the device at short circuit, which for inverted solar cells coincides with the burn-in phase reaching completion. At open circuit, device degradation is also correlated with an increase in lifetime of charge carriers under constant illumination conditions, an observation that may reflect an overall reduction in charge density within the solar cell. Characterising the cumulative effects of burn-in, we measure a c. 6% average reduction in PBDTTT-EFT:$PC_{71}BM$ absorbance above E_g. PDS measurements indicate that photobleaching of PBDTTT-EFT:$PC_{71}BM$ continues below the bandgap, however an increase in sub-bandgap absorbance for TiO_2 is found (a change that provides a mechanism for charge trapping at the cathode interface of the inverted solar cell). From ultra-fast TAS measurements, we do not observe differences in the kinetics of polaron formation and decay before and after burn-in, suggesting that the nanostructure of the polymer:fullerene blend remains relatively stable. A relatively long-lived PBDTTT-EFT GSB is however measured for degraded devices, which we tentatively attribute to the recombination of excited state species that do not form free carriers. Fabricating the device in a normal architecture, where both the anode and cathode interface layers have been replaced, does not impart significantly greater stability. Although normal architecture cells exhibit a greater initial efficiency (7.3% PCE on average, vs 6% PCE for inverted cells), both configurations lose more than 60% of these values after only 24 hours of light soaking under nitrogen. Because device degradation is apparently driven by light-mediated processes rather than elevated temperatures or high levels of oxygen and moisture exposure, our findings suggest a critical flaw in the current processing protocols of PBDTTT-EFT:$PC_{71}BM$ solar cells that emphasises initial PCE over long term stability.

To determine whether this blend holds promise as a semiconductor composition for practical OPV devices, we consider whether the severity of the burn-in phase can be reduced through cell design or alternative processing of the blend film. In Fig. 9, two methods are demonstrated for normal and inverted architecture devices.

For normal cells, the PBDTTT-EFT:$PC_{71}BM$ blend layer is cast from a chlorobenzene ink where the DIO additive has been substituted by 1,2-dichlorobenzene (DCB) as a co-solvent. Specifically, the volume composition of DCB in the ink is 50 vol%, considerably higher than DIO (3 vol%) in the reference processing protocol. The PCE for these devices is slightly lower (6.5 ± 0.4% vs 7.3 ± 0.5%, see Supporting Information Fig. S6 for details), however device stability is greatly improved with the severity of the burn-in phase reduced by approximately half. This result supports recent observations on the detrimental effects of DIO on the storage stability of PTB7 based OPV devices [31]. For inverted solar cells,

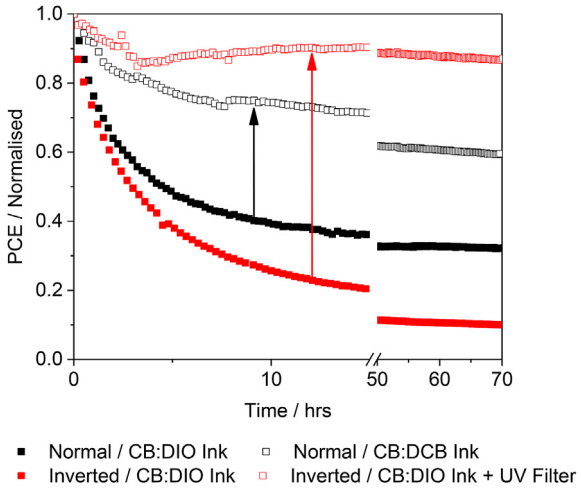

Fig. 9. Evolution of device efficiency under simulated solar illumination for PBDTTT-EFT:$PC_{71}BM$ reference solar cells (solid squares) and solar cells modified for reduced burn-in severity (open squares), normalised to their initial values.

placing a UV filter (435 nm long-pass) in front of the devices is also found to reduce the severity of the burn-in phase [49], highlighting the sensitivity of the device to short-wavelength illumination. These results are not intended to be exhaustive. Rather, they demonstrate how device stability can be improved through engineering routes instead of synthetic means, as well as motivating further studies on the role of casting solvent composition and UV light on solar cell degradation. Our results may have implications on the scale-up of other promising low-bandgap copolymers for high-performance organic photovoltaic devices, where device stability has yet to be determined. Work is currently underway to develop PBDTTT-EFT based photovoltaic devices with enhanced photostability, a prerequisite for evaluating thermal, oxygen and moisture tolerance.

4. Conclusions

We have presented a detailed study of burn-in behaviour in PBDTTT-EFT:$PC_{71}BM$ organic photovoltaic devices, a state-of-the-art system in the field with regard to initial power conversion efficiency. Measuring devices under nitrogen permits the limiting factors in stability to be identified. We find that for cells with the active layer processed according to current protocols, degradation from simulated solar illumination results in a rapid and severe burn-in phase where upwards of 60% of the initial device efficiency is lost within 24 hours continuous illumination. For inverted solar cells, in-situ transient electrical characterisation monitors the emergence of signatures attributed to charge trapping and an increase (at constant white light bias) in charge carrier lifetime, the kinetics for which are in close agreement with a reduction in J_{SC} and V_{OC} respectively. Performances losses are further correlated with a partial photobleaching of PBDTTT-EFT:$PC_{71}BM$, a small increase in sub bandgap absorbance in TiO_2 and a slower decay of the PBDTTT-EFT GSB, the latter observation identifying a possible channel for photocurrent loss at timescales not probed by our in-situ setup. PBDTTT-EFT:$PC_{71}BM$ solar cells are re-engineered with reduced burn-in phase severity, including substitution of DIO in the active layer casting solution, highlighting the complexity in the development of modern OPV devices where an encouraging initial performance does not necessarily imply promising stability.

Acknowledgements

The authors would like to thank SABIC for partially funding this research. PEH, EC and NCG thank the EPSRC for funding through the Supergen Supersolar Consortium (EP/J017361/1). PEH also thanks CKIK for additional funding. KD thanks the Gates Cambridge Scholarship fund. MAJ thanks Nyak Technology Ltd for PhD scholarship funding. AJP thanks David Lidzey (University of Sheffield) for use of a sample chamber for X-ray scattering measurements and Adam Brown (University of Cambridge) for UPS measurements.

Appendix A. Supplementary data

Supplementary data related to this article can be found at http://dx.doi.org/10.1016/j.orgel.2015.12.024.

The data underlying this publication are available at https://www.repository.cam.ac.uk/handle/1810/253106.

References

[1] G. Li, R. Zhu, Y. Yang, Nat. Phot. 6 (2012) 153–161.
[2] Z.C. He, C.M. Zhong, S.J. Su, M. Xu, H.B. Wu, Y. Cao, Nat. Phot. 6 (2012) 591–595.
[3] J.B. You, L.T. Dou, K. Yoshimura, T. Kato, K. Ohya, T. Moriarty, K. Emery, C.C. Chen, J. Gao, G. Li, Y. Yang, Nat. Commun. 4 (2013) 1446.
[4] M.A. Green, K. Emery, Y. Hishikawa, W. Warta, E.D. Dunlop, Prog. Photovolt. 22 (2014) 1–9.
[5] T. Wang, A.J. Pearson, D.G. Lidzey, J. Mater. Chem. C 1 (2013) 7266–7293.
[6] R.S. Kularatne, H.D. Magurudeniya, P. Sista, M.C. Biewer, M.C. Stefan, J. Polym. Sci. Pol. Chem. 51 (2013) 743–768.
[7] Z.G. Zhang, J.Z. Wang, J. Mater. Chem. 22 (2012) 4178–4187.
[8] M. Jorgensen, K. Norrman, S.A. Gevorgyan, T. Tromholt, B. Andreasen, F.C. Krebs, Adv. Mater 24 (2012) 580–612.
[9] H.L. Yip, A.K.Y. Jen, Energy Environ. Sci. 5 (2012) 5994–6011.
[10] K. Norrman, M.V. Madsen, S.A. Gevorgyan, F.C. Krebs, J. Am. Chem. Soc. 132 (2010) 16883–16892.
[11] M. Jorgensen, K. Norrman, F.C. Krebs, Sol. Energy Mat. Sol. C 92 (2008) 686–714.
[12] A. Tournebize, A. Rivaton, J.L. Gardette, C. Lombard, B. Pepin-Donat, S. Beaupre, M. Leclerc, Adv. Energy. Mater 4 (2014) 1301530.
[13] C.H. Peters, I.T. Sachs-Quintana, W.R. Mateker, T. Heumueller, J. Rivnay, R. Noriega, Z.M. Beiley, E.T. Hoke, A. Salleo, M.D. McGehee, Adv. Mater. 24 (2012) 663–668.
[14] J. Kong, S. Song, M. Yoo, G.Y. Lee, O. Kwon, J.K. Park, H. Back, G. Kim, S.H. Lee, H. Suh, K. Lee, Nat. Commun. 5 (2014) 5668.
[15] T.M. Clarke, C. Lungenschmied, J. Peet, N. Drolet, K. Sunahara, A. Furube, A.J. Mozer, Adv. Energy. Mater. 3 (2013) 1473–1483.
[16] C.H. Peters, I.T. Sachs-Quintana, J.P. Kastrop, S. Beaupre, M. Leclerc, M.D. McGehee, Adv. Energy. Mater 1 (2011) 491–494.
[17] A. Tournebize, P.O. Bussiere, P. Wong-Wah-Chung, S. Therias, A. Rivaton, J.L. Gardette, S. Beaupre, M. Leclerc, Adv. Energy. Mater. 3 (2013) 478–487.
[18] E. Bovill, N. Scarratt, J. Griffin, H. Yi, A. Iraqi, A.R. Buckley, J.W. Kingsley, D.G. Lidzey, Appl. Phys. Lett. (2015) 106.
[19] W.R. Mateker, I.T. Sachs-Quintana, G.F. Burkhard, R. Cheacharoen, M.D. McGehee, Chem. Mater. 27 (2015) 404–407.
[20] Z. Li, H.C. Wong, Z.G. Huang, H.L. Zhong, C.H. Tan, W.C. Tsoi, J.S. Kim, J.R. Durrant, J.T. Cabral, Nat. Commun. 4 (2013) 2227.
[21] H.C. Wong, Z. Li, C.H. Tan, H.L. Zhong, Z.G. Huang, H. Bronstein, I. McCulloch, J.T. Cabral, J.R. Durrant, ACS Nano 8 (2014) 1297–1308.
[22] F. Piersimoni, G. Degutis, S. Bertho, K. Vandewal, D. Spoltore, T. Vangerven, J. Drijkoningen, M.K. Van Bael, A. Hardy, J. D'Haen, W. Maes, D. Vanderzande, M. Nesladek, J. Manca, J. Polym. Sci. Pol. Phys. 51 (2013) 1209–1214.
[23] L.Y. Lu, L.P. Yu, Adv. Mater. 26 (2014) 4413–4430.
[24] S.J. Lou, J.M. Szarko, T. Xu, L. Yu, T.J. Marks, L.X. Chen, J. Am. Chem. Soc. 133 (2011) 20661–20663.
[25] F. Liu, W. Zhao, J.R. Tumbleston, C. Wang, Y. Gu, D. Wang, A.L. Briseno, H. Ade, T.P. Russell, Adv. Energy. Mater. 4 (2014) 1301377.
[26] G.J. Hedley, A.J. Ward, A. Alekseev, C.T. Howells, E.R. Martins, L.A. Serrano, G. Cooke, A. Ruseckas, I.D.W. Samuel, Nat. Commun. 4 (2013) 2867.
[27] H.C. Liao, C.C. Ho, C.Y. Chang, M.H. Jao, S.B. Darling, W.F. Su, Mater. Today 16 (2013) 326–336.
[28] I.P. Murray, S.J. Lou, L.J. Cote, S. Loser, C.J. Kadleck, T. Xu, J.M. Szarko, B.S. Rolczynski, J.E. Johns, J.X. Huang, L.P. Yu, L.X. Chen, T.J. Marks, M.C. Hersam, J. Phys. Chem. Lett. 2 (2011) 3006–3012.
[29] J.B. You, C.C. Chen, L.T. Dou, S. Murase, H.S. Duan, S.A. Hawks, T. Xu, H.J. Son, L.P. Yu, G. Li, Y. Yang, Adv. Mater. 24 (2012) 5267–5272.
[30] Y. Wu, W. Zhang, X. Li, C. Min, T. Jiu, Y. Zhu, N. Dai, J. Fang, ACS Appl. Mater. Interfaces 5 (2013) 10428–10432.
[31] W. Kim, J.K. Kim, E. Kim, T.K. Ahn, D.H. Wang, J.H. Park, J. Phys. Chem. C 119 (2015) 5954–5961.
[32] S.Q. Zhang, L. Ye, W.C. Zhao, D.L. Liu, H.F. Yao, J.H. Hou, Macromolecules 47 (2014) 4653–4659.
[33] L. Ye, S.Q. Zhang, W.C. Zhao, H.F. Yao, J.H. Hou, Chem. Mater. 26 (2014) 3603–3605.
[34] http://www.1-material.com/wp-content/uploads/2013/12/1M_From-PTB7-to-PCE-10_Confidential.pdf
[35] L.L. Chang, H.W.A. Lademann, J.B. Bonekamp, K. Meerholz, A.J. Moule, Adv. Funct. Mater. 21 (2011) 1779–1787.
[36] L. Ye, Y. Jing, X. Guo, H. Sun, S.Q. Zhang, M.J. Zhang, L.J. Huo, J.H. Hou, J. Phys. Chem. C 117 (2013) 14920–14928.
[37] I. Hwang, C.R. McNeill, N.C. Greenham, J. Appl. Phys. 106 (2009) 094506.
[38] Z. Li, F. Gao, N.C. Greenham, C.R. McNeill, Adv. Funct. Mater. 21 (2011) 1419–1431.
[39] F. Gao, Z. Li, J.P. Wang, A. Rao, I.A. Howard, A. Abrusci, S. Massip, C.R. McNeill, N.C. Greenham, ACS Nano 8 (2014) 3213–3221.
[40] Z. Li, C.R. McNeill, J. Appl. Phys. 109 (2011) 074513.
[42] B.J.T. de Villers, R.C.I. MacKenzie, J.J. Jasieniak, N.D. Treat, M.L. Chabinyc, Adv. Energy. Mater. 4 (2014) 1301290.
[43] T. Heumueller, W.R. Mateker, I.T. Sachs-Quintana, K. Vandewal, J.A. Bartelt, T.M. Burke, T. Ameri, C.J. Brabec, M.D. McGehee, Energy Environ. Sci. 7 (2014) 2974–2980.
[44] D. Credgington, J.R. Durrant, J. Phys. Chem. Lett. 3 (2012) 1465–1478.
[45] D. Credgington, R. Hamilton, P. Atienzar, J. Nelson, J.R. Durrant, Adv. Funct. Mater. 21 (2011) 2744–2753.
[46] C.G. Shuttle, A. Maurano, R. Hamilton, B. O'Regan, J.C. de Mello, J.R. Durrant, Appl. Phys. Lett. 93 (2008) 183501.
[47] X.G. Guo, N.J. Zhou, S.J. Lou, J. Smith, D.B. Tice, J.W. Hennek, R.P. Ortiz, J.T.L. Navarrete, S.Y. Li, J. Strzalka, L.X. Chen, R.P.H. Chang, A. Facchetti, T.J. Marks, Nat. Phot. 7 (2013) 825–833.
[48] F. Deschler, A. De Sio, E. von Hauff, P. Kutka, T. Sauermann, H.J. Egelhaaf, J. Hauch, E. Da Como, Adv. Funct. Mater. 22 (2012) 1461–1469.
[49] T. Leijtens, G.E. Eperon, S. Pathak, A. Abate, M.M. Lee, H.J. Snaith, Nat. Commun. 4 (2013) 2885.
[50] J. Razzell-Hollis, J. Wade, W.C. Tsoi, Y. Soon, J. Durrant, J.S. Kim, J. Mater. Chem. A 2 (2014) 20189–20195.